STRUCTURE OF THE CELL ENVELOPE OF *HALOBACTERIUM HALOBIUM*

ALLEN E. BLAUROCK, WALTHER STOECKENIUS,
DIETER OESTERHELT, and GERRIT L. SCHERPHOF

From the Cardiovascular Research Institute, University of California at San Francisco, San Francisco, California 94143. Dr. Blaurock's present address is the Division of Chemistry and Chemical Engineering, California Institute of Technology, Pasadena, California 91125. Dr. Oesterhelt's present address is the Institut für Biochemie, der Universität Würzburg, 87 Würzburg, West Germany. Dr. Scherphof's present address is the State University of Groningen, Laboratory of Physiological Chemistry, Groningen, The Netherlands.

ABSTRACT

The structure of the isolated cell envelope of *Halobacterium halobium* is studied by X-ray diffraction, electron microscopy, and biochemical analysis. The envelope consists of the cell membrane and two layers of protein outside. The outer layer of protein shows a regular arrangement of the protein or glycoprotein particles and is therefore identified as the cell wall. Just outside the cell membrane is a 20 Å-thick layer of protein. It is a third structure in the envelope, the function of which may be distinct from that of the cell membrane and the cell wall. This inner layer of protein is separated from the outer protein layer by a 65 Å-wide space which has an electron density very close to that of the suspending medium, and which can be etched after freeze-fracture. The space is tentatively identified as the periplasmic space.

At NaCl concentrations below 2.0 M, both protein layers of the envelope disintegrate. Gel filtration and analytical ultracentrifugation of the soluble components from the two protein layers reveal two major bands of protein with apparent mol wt of ~16,000 and 21,000. At the same time, the cell membrane stays essentially intact as long as the Mg^{++} concentration is kept at ≥ 20 mM. The cell membrane breaks into small fragments when treated with 0.1 M NaCl and EDTA, or with distilled water, and some soluble proteins, including flavins and cytochromes, are released. The cell membrane apparently has an asymmetric bilayer structure, with substantial amounts of protein penetrating the hydrophobic core of the lipid bilayer.

Recent studies of the envelope of Halobacteria species have taken advantage of its easy disintegration: when the concentrated saline of the growth medium is diluted, the envelope disintegrates into soluble proteins and membrane fragments. Intact cells, isolated envelopes, and the disintegration products have been investigated by electron microscopy and related chemical studies (14, 29, 30, 43–45).

In this way, it has been shown that there is a cell wall. It contains only protein with small amounts of carbohydrate, probably in the form of glycopro-

tein (25). Thus, unlike that of many procaryotic cells, the envelope contains neither peptidoglycans (muramic and diaminopimelic acids) nor teichoic acids (26–28). The lipids are apparently confined to the cell membrane, for there are no lipid-containing intracytoplasmic membranes. One large fragment of the cell membrane, the purple membrane, has been shown to contain only one species of protein molecule, resembling the visual pigments, embedded in the membrane in a planar crystalline array (9, 10, 35). The purple membrane apparently functions as a light energy transducer (16, 36, 40).

We now report X-ray diffraction and freeze-etch experiments giving a more detailed picture of the envelope of *Halobacterium halobium*. Its envelope structure bears a general resemblance to that of other bacteria. As expected from the chemistry, however, there are important differences. Our observations demonstrate within the envelope, between the cell membrane and the wall, a layer which has the same electron density as the surrounding saline and which can be etched after cross-fracture. This layer has been tentatively identified with the periplasmic space postulated for some gram-negative bacteria. The outer protein layer of the envelope is about 40 Å thick. Separated from it by the presumed periplasmic space is a second, thinner layer of protein, located just outside the cell membrane. This layer has not been characterized chemically nor is its function known. The soluble proteins released upon disintegration of the envelope have been partially characterized chemically. We find two major protein bands with apparent mol wt of 16,000 and 21,000; the possibility that these are proteolytic fragments has not been eliminated. Our data confirm bilayer structure for the cell membrane and suggest some structural asymmetry.

MATERIALS AND METHODS

Bacteria and Culture Conditions

H. halobium R_1 is a spontaneous mutant of *H. halobium* NRL (44), which has lost the ability to form gas vacuoles; it was used in most experiments. Occasionally, the wild type NRL strain was used for some experiments and gave essentially the same results; the gas vacuole membranes present in the wild type do not contain lipids (44). Cells are grown at 39°C on complex medium in a 14-liter fermentor (Microferm, New Brunswick Scientific Co., Inc., New Brunswick, N.J.) with vigorous aeration and under constant illumination as previously described (45). The inoculum consists of 300 ml late exponential phase cells; the culture reached stationary phase in about 70 h.

Preparation and Fractionation of Cell Envelopes

Cells from 10 liters of a stationary phase culture are harvested by centrifugation at 20,000 *g* for 5 min and suspended in 500 ml of "basal salt" (BS = 2.0 g of KCL, 3.0 g of sodium citrate · 2 H_2O, 20.0 g of $MgSO_4 \cdot 7\ H_2O$, 250.0 g of NaCl in 1,000 ml of deionized water). The cells are collected in a plastic container which is then placed in liquid nitrogen; the liquid N_2 is then allowed to evaporate. This procedure results in the breakage of virtually all cells.

In earlier work, shaking with glass beads in a Bronwill disintegrator was used to break the cells (45). Several other methods, e.g. the use of a high speed blender or a French press, also were tried, but all were found less satisfactory than the slow freezing and thawing, which does not take long and leaves no intact cells. It should be noted that rapid freezing by pouring the cell suspension into liquid nitrogen gave poorer results.

When the suspension of broken cells has again reached room temperature, it is stirred for 1 h with 5 mg of DNase added (Worthington Biochemical Corp., Freehold, N. J.) to overcome the high viscosity of the suspension. The envelopes, which reform closed structures, are harvested by centrifugation at 20,000 *g* for 2 h.

The resulting crude envelope fraction is suspended in 300 ml of BS and again centrifuged at 100,000 *g* for 30 min. This step is repeated, usually three times, until only small and constant amounts of protein are found in the supernate. This preparation of envelopes is designated E-BS.

Most of the cytoplasm and soluble material is removed with the supernate in the first centrifugation of the suspension. The pellet is deep red while the supernate at this stage appears clear with a light orange color, indicating that little envelope material remains in suspension; the orange color results from yellow soluble cytoplasmic material and small envelope fragments of pink color. The following sedimentations remove little additional material from the pellet (see Table I). If the purified envelopes in the pellet are frozen and thawed again, sedimentation under the same conditions yields very little additional protein in the supernate. A third freezing, thaw-

TABLE I

Protein Determination in the Supernate of Cell Envelopes

	Centrifugation				
	1st	2nd	3rd	4th	5th
Protein (g) in supernate	4.40	0.33	0.09	0.07	0.06

Cells from a 10-liter culture are frozen, thawed, and centrifuged as described under Materials and Methods. Total protein in the supernate was determined (Lowry).

ing, and sedimentation has practically no effect on the composition of the envelope pellet.

E-BS from a 10-liter culture is incubated at room temperature for 1 h in a total vol of 200 ml of H_2O containing 20 mM $MgSO_4$, 10 mM Tris buffer, pH 8.0, and varying concentrations of NaCl. After sedimentation for 30 min at 100,000 *g*, the sediment is resuspended in the same solution and sedimented again. The combined supernates typically have a very light pink color resulting from small particulate envelope components; these can be removed by prolonged centrifugation. The sedimented fractions thus obtained are termed E-2.0, E-1.8, ··· E-0.1, according to the molarity of NaCl used. E-Mg designates a fraction that was resuspended in 20 mM $MgSO_4$; E-0.1/EDTA is derived from E-0.1 by dialyzing it against 0.1 M EDTA, pH 7.0, in 0.1 M NaCl. Centrifugation time and speed are increased to 5 h at 300,000 *g* in this step. E-H_2O is prepared by dialyzing E-0.1/EDTA against H_2O and centrifuging at 50,000 *g* for 30 min to remove the purple membrane. The sediment is resuspended in water and centrifuged again. The combined supernates are centrifuged at 100,000 *g* until a colorless supernate and a red pellet are obtained. If the centrifugation time is relatively short and the cells contain considerable amounts of residual purple membrane, this membrane may be concentrated in this fraction. The red pellet resuspended in water is E-H_2O. A fraction indistinguishable from E-H_2O may be prepared by dialyzing E-BS or E-1.0 directly against water, centrifuging, and resuspending in water. E-H_2O is thus equivalent to the red membrane fraction (44). Concentration of the supernates is carried out with an Aminco Diaflow cell (American Instrument Co., Inc., Silver Springs, Md.).

X-Ray Diffraction

A specimen of intact cells, isolated envelopes, or one of the envelope fractions is made by centrifuging for 1 h at 400,000 *g* and then drawing material from the pellet into a thin-walled glass capillary (Pantak; Uni-Mex Caine). The capillary is flame-sealed inside a larger capillary. The diameter of the inner capillary is 0.5 mm for specimens in concentrated saline, which absorbs X rays more strongly than water, or else 1.0 mm for specimens in dilute salt solutions. The specimen is examined in the polarizing microscope and, if possible, a uniformly birefringent region is chosen for exposure. The X rays from a Jarrell-Ash microfocus generator (Jarrell-Ash Div., Fisher Scientific Co., Waltham, Mass.) with a copper target are predominantly of wavelength $\lambda = 1.542$ Å. The low-angle point-focusing diffraction camera is described elsewhere (7, 9, 18). Exposures are carried out at room temperature and generally last 24 h. The specimen-to-film distance is either 8–9 cm to record particularly the very low-angle diffraction or 4 cm to increase the photographic film density. Densities on the Ilford Ilfex film are measured with a Joyce-Loebl Mark III CS recording microdensitometer (Joyce, Loebl and Co., Inc., Burlington, Mass.). After subtracting a constant value for background (9), the densitometer traces are corrected for disorientation by multiplying the density at a given radius, I_R, times the square of the radius, R^2 (48). For any point on the continuous diffraction pattern, the Bragg's law spacing corresponding to the diffraction angle, θ, is $\lambda/(2 \sin [\theta/2]) \equiv 2\pi/k$. Following common practice, the Bragg's law spacing is given rather than the diffraction angle. For spacings >15 Å the Bragg's law spacing is to a good approximation proportional to $1/R$.

Electron Microscopy

The techniques used for shadowed and sectioned preparations have been described previously (45). For freeze-fracturing and freeze-etching, a Balzers BA 510 unit is used, essentially as described by Moor and Mühlethaler (34). Generally, no cryoprotective agents are employed. The preparations are viewed in a Siemens Elmiskop 1 or 101.

RESULTS

X-Ray Diffraction

THE CELL ENVELOPE PATTERN: The X-ray diffraction pattern from unoriented dispersions of either intact cells or isolated envelopes in BS includes three concentric, narrow bands. With sufficient exposure, there is also a broader band outside; this band is centered at a Bragg's law spacing of 21 Å. When a birefringent region of the capillary specimen is exposed, the bands are seen as diffuse arcs all most intense along one axis, labeled M (for meridian) in Fig. 1*a*. Both the birefringence and the oriented diffraction show that in this case the envelopes have some net orientation.

The pair of corrected intensity curves in Fig. 2, shown out to a Bragg's law spacing of 30 Å, is from the exposure of Fig. 1*a*. The curve labeled M in Fig. 2 is much the same as the corrected radial intensity from the unoriented cells or envelopes. The small, regular separation of the three bands in Fig. 2 indicates a structure with an overall thickness of at least 150 Å (see below). The partially oriented specimens have not been sufficiently exposed to provide an accurate difference curve covering the 21 Å band.

The bands are identified in the following way as diffraction from the envelope profile, i.e. from the average curve of electron density along a line at right angles to the plane of the envelope. In the diffraction patterns from birefringent specimens, the three closely spaced diffuse arcs and the broader one at 21 Å all have the same orientation. With sufficient exposure there is also a series of sharp reflections; the strongest of these are seen in

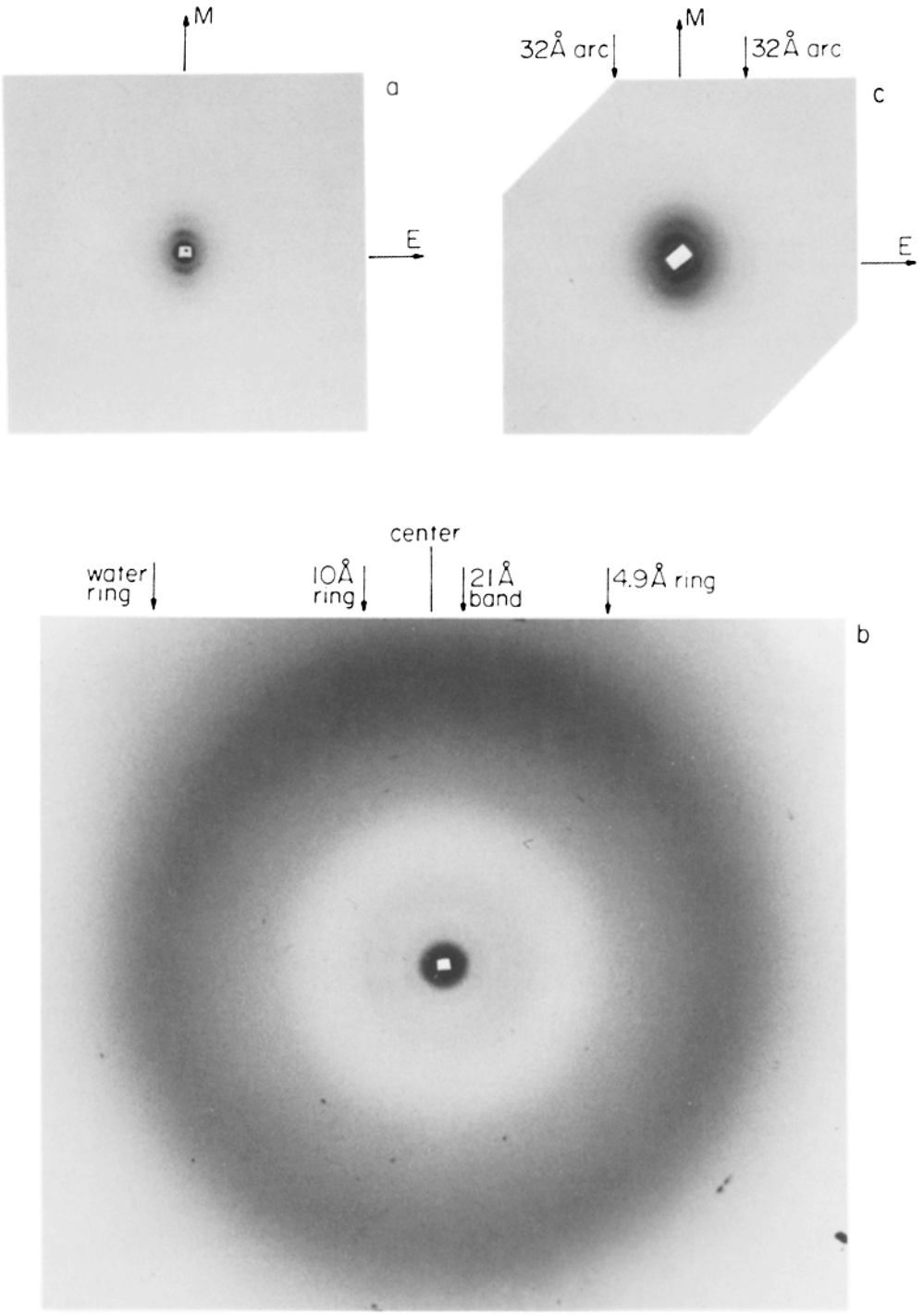

FIGURE 1 Low-angle X-ray diffraction patterns from the isolated envelope in basal salts (E-BS). (*a*) The darkest arc on the vertical axis, labeled M, corresponds to the peak at 100 Å in Fig. 2. The diffraction is not very strong because the X rays are strongly absorbed by the BS. 25.7-h exposure; 8.9 cm from specimen to film. (*b*) The intensity is greater than in (*a*) because the specimen to film distance, 3.7 cm, is considerably shorter. There is very little orientation in this exposure. The 21 Å-band is visible just outside the more intense diffraction in the region shown in (*a*). The diffuse ring at 4.9 Å is attributed to the lipids in the cell membrane and the ring at 10 Å, to protein. 65.5-h exposure. (*c*) Similar to (*a*), except that the orientation is less good. The faint, sharp arcs are in-plane reflections from the purple membrane in the envelope (see also Fig. 3*c*). 26.1-h exposure; 9.5 cm from specimen to film. (We regret that the arrows indicating the centers of the diffraction patterns and the Bragg spacings of the reflections are not correctly aligned in some cases. In these cases, the arrows and center lines are all off-center by the same amount, and hence the *scale* of Bragg spacings is still correct. Note added at the request of the authors.)

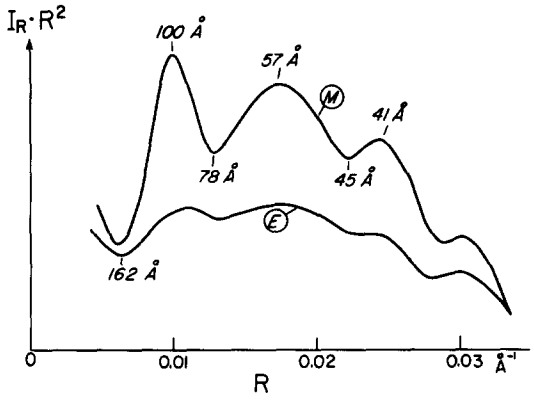

FIGURE 2 A pair of corrected densitometer tracings of the envelope in BS. $I_R R^2$ is plotted vs. R, the distance from the center of the pattern. M and E are tracings along the respective axes on the exposure of Fig. 1*a*. The Bragg's law spacings are given for the centers of the peaks and troughs. The difference M minus E (omitted for the sake of clarity) is the profile diffraction. The small peak in both M and E at 0.03 $Å^{-1}$ is not due to the envelope profile because it is not oriented. Its origin is not known.

Fig. 1*c*. They are identified by their Bragg's law spacings and their intensities as in-plane diffraction from the patches of purple membrane which form part of the cell membrane in these envelopes (10). The sharp rings are most intense along the axis E (for equator), which is therefore parallel to the plane of the cell membrane. Thus, M is at right angles to the plane of the membrane, and hence at right angles to the plane of the envelope.

Electron micrographs of shadowed whole bacteria and of intact envelopes show a highly ordered structure on the surface of the cells (21, 45). This wall structure should give rise to a series of sharp, in-plane X-ray reflections beginning at a Bragg's law spacing of about 130 Å, but no such series is observed. The absence of the expected series may be due in part to the comparatively weak exposure, but it also indicates a rather small variation of electron density in the plane, so that the expected X-ray reflections will be weak. The protein molecules composing the wall may be closely packed in a uniform layer. Alternatively, the electron-dense saline may fill indentations or pores in the wall. Unoriented specimens were the first to be exposed, and the possibility was considered that the in-plane wall structure might be disordered in such a way as to give rise to the observed diffuse reflections. Later, the oriented specimens were prepared and this possibility was ruled out because these reflections are not oriented in the plane of the wall.

The wide-angle diffraction from the envelopes (E-BS) includes three prominent, diffuse rings (Fig. 1*b*). A diffuse ring at 10 Å is attributed to the protein (17) since the extracted lipids do not give a ring at 10 Å (9). A diffuse ring at 4.9 Å is attributed to the lipids in the membrane since a similar ring is present in the pattern of the lipids extracted from both the red and purple membranes (9). An additional contribution from the protein near 5 Å also is possible (17). A diffuse ring at about 3 Å is attributed to the water.

As the salt concentration is lowered in steps from 4.3 to 2.0 M, the three closely spaced bands in Fig. 2 are attenuated. We note that this treatment causes intact cells to take irregular shapes, indicating that the wall has been disturbed (1, 33). The wall material is still present (see Biochemical Analysis section of Results), and we attribute the attentuation to a disordering of the envelope structure. At NaCl concentrations below 2.0 M, wall material is lost from the envelopes (reference 44; see also Biochemical Analysis), and the three closely spaced reflections are lost altogether from the diffraction pattern. The 21-Å band persists. In place of the three closely spaced reflections, a single broad band appears, as in the red membrane diffraction pattern (Fig. 4).

THE RED MEMBRANE PATTERN AND ITS INTERPRETATION: The pelleted red membrane preparation (44, 45), E-H_2O, gives continuous low-angle X-ray intensity including two broad bands. For E-H_2O, or E-H_2O resuspended in dilute saline,[1] the bands are centered at Bragg's law spacings of 42 Å and 21 Å (Fig. 4*a*). When a birefringent region in a capillary specimen is exposed, both bands are oriented in the same direction. The first band is visible in Fig. 3*a*. A pair of corrected intensity curves is shown in Fig. 4*a*. Diffuse rings at 10 Å and 4.9 Å are attributed to the membrane protein and lipids (Fig. 3*b*), respectively.

When much, but not all, of the water was allowed to evaporate from a capillary specimen, the more concentrated membranes showed a uniform birefringence, and X-ray exposure gave a series of

[1] The red membrane sediments much more readily in dilute saline. The salt presumably shields charged sites in the membrane.

fairly sharp arcs oriented parallel to the capillary axis. The arcs are clearly profile diffraction: their Bragg's law spacings of 94 Å/h, h = 1, 2, 3 indicate stacking with one membrane every 94 Å; for a stack of thin sheets, the arcs are oriented at right angles to the plane of the sheets. The integrated, corrected intensities of the three arcs have been fitted between the pair of continuous curves found for the more dilute dispersion (Fig. 4*a*). The fit, while not exact, is close enough to show that the oriented bands also are profile diffraction.

The purple membrane is still present in E-0.1/EDTA. In Fig. 3*c*, the sharp in-plane reflections from this membrane are oriented at right angles to the broad band, confirming that the band is profile diffraction.

When the red membrane fraction (E-H_2O) is resuspended in the electron-dense BS, the diffraction pattern changes. The center of the first broad band in the corrected tracing (Fig. 4*b*) is shifted from 42 Å to 50 Å and the first intensity minimum is shifted from about 100 Å (0.01 Å^{-1}) to a position too close to the center to be observed. The second broad band, however, remains at 21 Å. As will become clear, these observations are the predictable effects of increasing the electron density of the fluid surrounding a bilayer membrane.

The low-angle diffraction pattern from the red membrane is of the kind characteristic of lipid bilayers (41, 48) and has also been observed from several other biological membranes (9, 10, 48). Interpreted in terms of a bilayer profile, the two broad bands in Fig. 4*a*, which are centered at Bragg's law spacings of 42 Å/h, h = 1 and 2, indicate two electron-dense layers centered about 40 Å apart. If the core of the bilayer, the region between the electron-dense layers, had the same average electron density as the surrounding fluid, the first minimum would be centered at a Bragg's law spacing of about 80 Å.[2] The position of the first minimum in Fig. 4*a*, at a Bragg's law spacing near 100 Å, therefore indicates that the average electron density in the core of the red membrane is less than in the surrounding 0.1 M NaCl.[2] When the red membrane is transferred to the more electron-dense BS, the density in the core will be relatively lower and the first minimum is predicted to shift closer to the origin (8). The shift noted above therefore confirms the bilayer interpretation. Constant membrane structure is indicated by the second broad band remaining at 21 Å.

For the red membrane in dilute saline (Fig. 4*a*), the difference M minus E goes to a minimum near 100 Å and again near 25 Å (0.04 Å^{-1}). A symmetric bilayer profile would give zero difference at both points. The nonzero minima observed therefore suggest an asymmetric bilayer. At the same time, however, the low values at the two minima limit the asymmetry possible (9).

We have calculated electron density profiles from the diffraction patterns of the red membrane fraction (E-H_2O) in 0.1 M NaCl and in BS by choosing the phase angles for a symmetric bilayer (Fig. 5). Assuming that the asymmetry is small, the average of the two asymmetric halves of the correct profile will be closely approximated by half of the calculated profile. Halves of the calculated low-resolution profiles are superimposed on the right of Fig. 5. The higher electron density of the BS outside the bilayer is correctly shown, satisfying a strong test of the bilayer interpretation. The comparison also provides a scale of electron density. Half of a higher resolution profile of the red membrane in 0.1 M NaCl is shown on the left of Fig. 5. The central trough in the low- or high-resolution profile must locate lipid hydrocarbon chains, since the lipid headgroups and the protein are both considerably more electron dense than 0.1 M NaCl.

CELL MEMBRANE PROFILE: A bilayer profile for the cell membrane is indicated by the crystallographic Patterson function (Fig. 6), which is calculated from the corrected diffraction pattern with no assumption about the structure (22). This function is a correlation function; it measures the distances between parts of the structure, appropriately weighted. The form of the solid curve in Fig. 6, from the origin out to 50 Å, is familiar from the Patterson functions for nerve myelin (4) and the retinal outer segment disks (11). For both of these membranes, a bilayer profile has been confirmed. The minimum at 25 Å is attributed to correlation of the bilayer peaks with the trough between them and the subsidiary peak at 45 Å, to correlation of the peaks with each other. There is also a more direct confirmation, as follows.

Centered at 145 Å in Fig. 6 is an image of the cell membrane due to the correlation of the outer protein layer with the membrane and an adjacent inner protein layer (see below). Because of the appreciable thickness of the outer protein layer,

[2] These points can be verified on Fig. 5 in reference 48. Note that the curves there must first be squared.

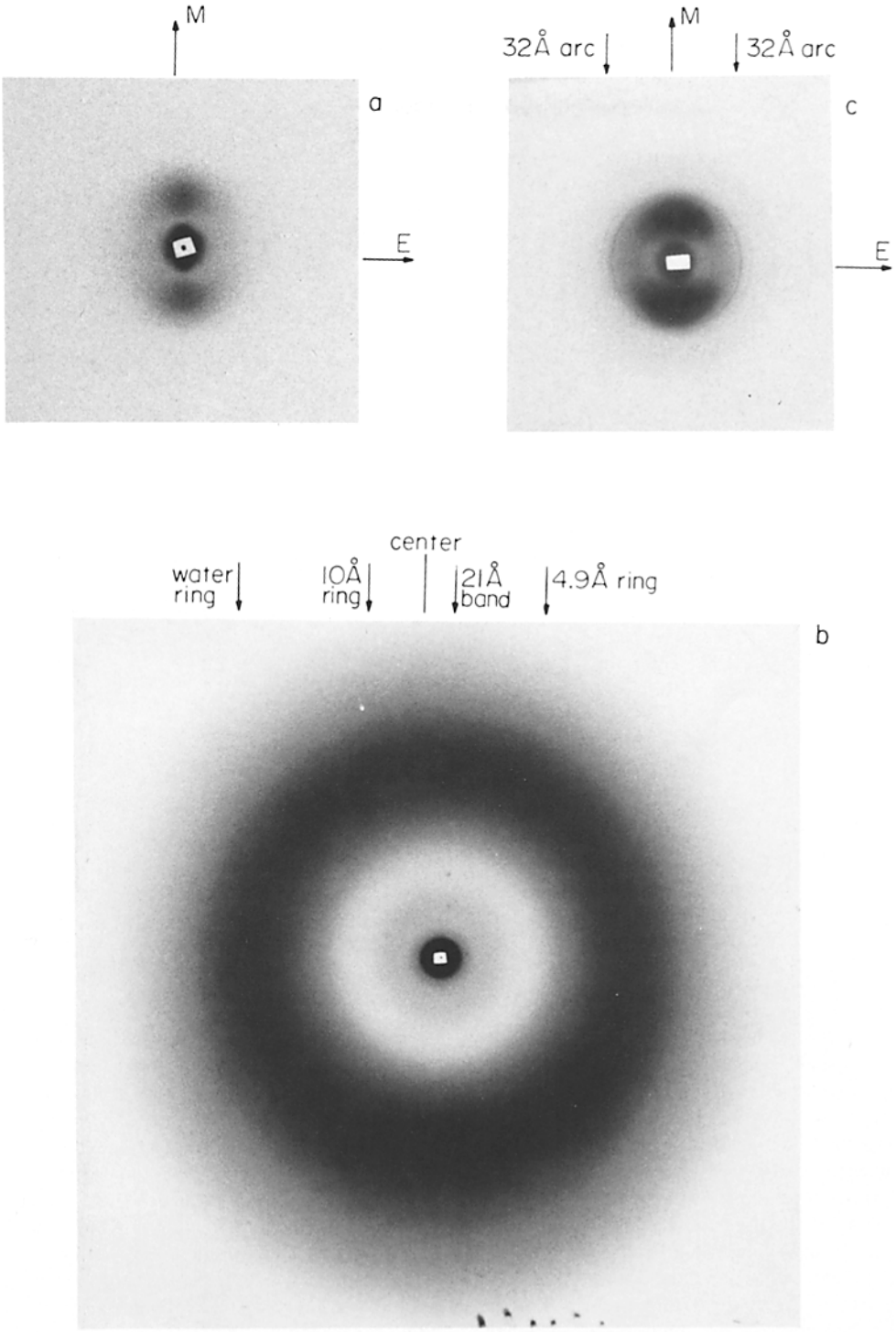

FIGURE 3 Low-angle X-ray pattern from the wall-free red membrane. (*a*) The red membrane (E-H_2O) in 0.1 M NaCl. The dark band on the vertical axis corresponds to the peak at 42 Å in M, Fig. 4*a*. The 21 Å-band is visible on the original negative. 5-h exposure; 7.3 cm from specimen to film. (*b*) Same as in (*a*), but at a shorter specimen-to-film distance, 2.7 cm. There is very little orientation in this exposure. The 21 Å-band is visible just outside the 42 Å-band, which is overexposed here. The diffuse ring at 4.9 Å is attributed to the membrane lipids and the ring at 10 Å, to protein. 11.8-h exposure. (*c*) In 0.1 M NaCl and 0.1 M EDTA, pH 8.0 (E-0.1/EDTA). The vertical axis is similar to (*a*). The pair of sharp arcs on the horizontal axis, the equator, is the strongest in-plane reflection from the purple membrane, i.e. the (1,1)-reflection at 32 Å. Other in-plane reflections from the purple membrane are visible on the original negative. 22.1-h exposure; 9.5 cm from specimen to film. (Refer to explanation in Fig. 1 about alignment of arrows.)

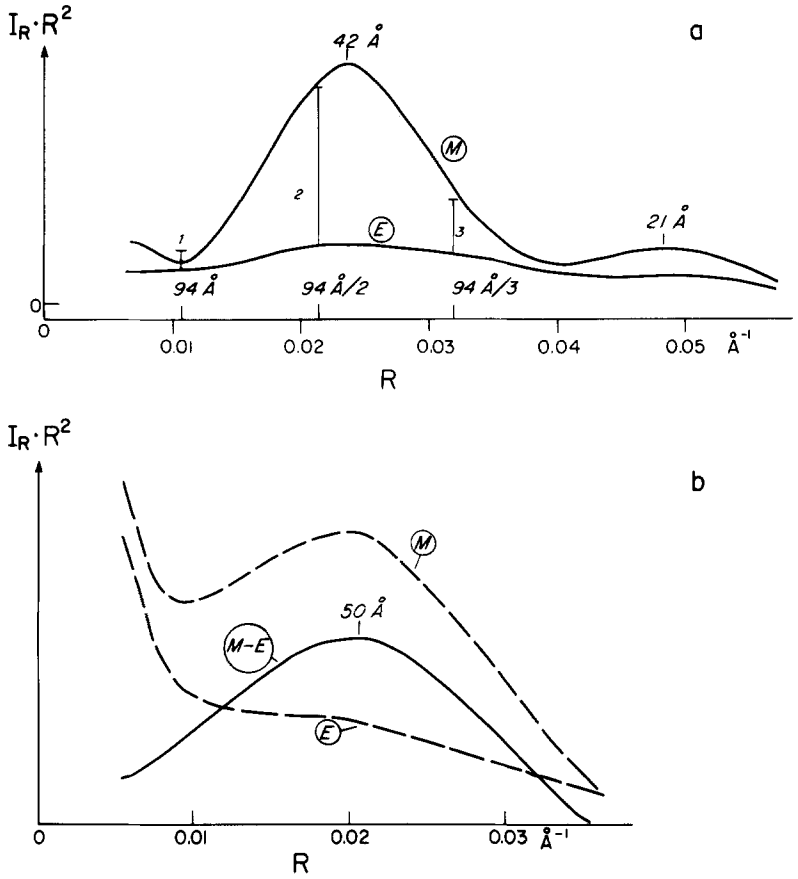

FIGURE 4 Corrected densitometer tracings of two patterns of the red membrane. (*a*) In 0.1 M NaCl, there are broad bands centered at 42 Å and 21 Å. For clarity, the difference curve *M-E* is omitted. Exposure of Fig. 3*a*. (*b*) In basal salts. The difference curve *M-E* (——) shows a broad band centered at 50 Å. The pattern is too weak to provide an accurate difference curve over the 21 Å band. The strong central scatter seen in both *M* and *E* is not always present.

the resolution in this image is limited. Nonetheless, a bilayer-like profile is clearly seen centered at 145 Å. The central minimum is expected because the lipid fatty chains located in the core of a bilayer membrane will contrast negatively with the BS while the outer protein layer will be positive. The broad peak at 106 Å is attributed to the correlation of the outer protein layer with both a layer of electron-dense lipid headgroups near the extracellular surface of the membrane and the inner protein layer; the two are unresolved because the outer protein layer is so broad. The shoulder at 165 Å is attributed to correlation with the second layer of lipid headgroups, near the cytoplasmic surface of the membrane.

ANALYSIS OF THE ENVELOPE PATTERN: A picture of the envelope in cross section (Fig. 8) has been developed as follows. Comparing the respective diffraction patterns from the envelope in BS (Fig. 2) and from the wall-free red membrane in BS (Fig. 4*b*), it appears that the wall introduces a series of closely spaced peaks and troughs into the red membrane pattern. This interpretation is confirmed by the complete loss of peaks and troughs just when the wall disintegrates. The series dies out near 0.025 Å^{-1}. Beyond, strong exposures of both patterns show a minimum of intensity near 25 Å and a broad band centered at 21 Å (Figs. 1*b* and 3*b*). Thus, only the diffraction from the cell membrane is evident beyond 0.025 Å^{-1}.

Assuming that the envelope consists of the cell membrane parallel to the cell wall, the expected profile diffraction can be expressed as a sum of

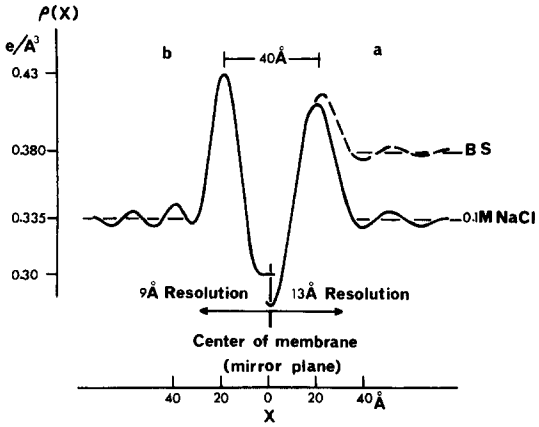

FIGURE 5 Approximate, bilayer profiles for the red membrane (see text). For economy, only half of each symmetric profile is shown. A period of 150 Å was chosen in order to carry out the calculations. (*a*) To the right of center are halves of the two symmetric Fourier syntheses calculated by using the square roots of the difference curves in Fig. 4: (——), in 0.1 M NaCl; and (---), in BS. The bilayer phase angles were 0 from the center out to the first minimum in Fig. 4*a* and then π out to the second minimum (0.04 $Å^{-1}$). The resolution is 13 Å. (*b*) The half-profile to the left of the center (——) uses data from the 21 Å diffraction band in Fig. 4*a* as well. The phase angle was 0 over the second band. This value has not yet been confirmed. The resolution is 9 Å.

three patterns (6): (*a*) a profile pattern from the membrane alone; (*b*) a profile pattern from the wall alone; and (*c*) a pattern due to cross interference between the membrane and the wall. Assuming that the cell membrane dominates, i.e., that contribution (*b*) is small, the cell wall will reveal itself mainly through the cross interference. Contribution (*c*) is, then, of particular interest. The mathematical expression derived for (*c*) is:

$$M\ W \cos\left(\frac{4\ \pi \sin\ (\theta/2)}{\lambda}\ S\right), \qquad (1)$$

where M and W are the Fourier transforms of the cell membrane and cell wall profiles, respectively, and S is the center-to-center distance between them (6). For small angles of diffraction, sin $(\theta/2)$ varies nearly linearly with θ, and hence the cosine factor in Eq. 1 implies a regular succession of peaks and troughs. The amplitudes of these will be modified from those of the cosine because M and W also will vary with θ. Nonetheless, it may be possible to estimate the distance S from the frequency of the peaks and troughs in the diffraction pattern and the thickness of the wall from the Bragg's law spacing at which they die out as W goes to zero. An example of the expected diffraction is shown in Fig. 7*b*. The

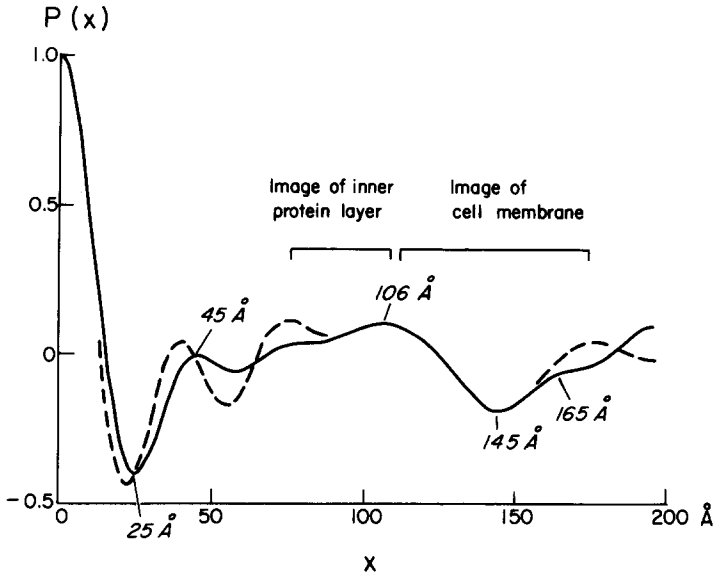

FIGURE 6 The Patterson function (——) computed without assumption using data from Fig. 2. A period of 393 Å was chosen to do the calculations. Centered at 145 Å is an image of the cell membrane. The dashed curve (----) shows the Patterson function computed from the solid curve in Fig. 7*b*. Both curves are to the same resolution, 13 Å.

validity of the theory has been confirmed by adding cytochrome c to the surface of an artificial lipid bilayer membrane (7).

The distance S and the wall thickness are deduced from Fig. 2 as follows. The difference M-E has been identified above as profile diffraction. The closely spaced peaks and troughs in Fig. 2 are centered approximately at 145 Å/h: troughs at 160 Å ($h \simeq 1$); 78 Å ($h \simeq 2$) and 45 Å ($h \simeq 3$); peaks at 100 Å ($h \simeq 3/2$), 57 Å ($h \simeq 5/2$) and 41 Å ($h \simeq 7/2$). Thus, the separation of successive peaks, and of successive troughs, indicates that S is about 145 Å. Because the spacings 145 Å/h, $h = 1$, 2 and 3, all locate troughs, quite dissimilar profiles are indicated for the two parts of the envelope: identical or similar profiles generally would give peaks, not troughs, at or near the integer sub multiples of 145 Å.[3]

In Fig. 2, all but the first of the troughs in M are well above E. This observation, together with the 21 A band common to both envelope and red membrane patterns, indicates that the cell membrane dominates the envelope profile diffraction beyond 0.01 Å^{-1}, and that the wall is revealed largely by a cross-interference effect which dies out near 0.025 Å^{-1} (40 Å). This conclusion is consistent with the finding that the cell membrane accounts for a substantial part of the dry weight of the envelope (see Biochemical Analysis). Because there are no closely spaced peaks in the difference curve M-E beyond 40 Å, the wall thickness is about 40 Å on average. If S varies substantially with time, or from place to place, the peaks will die out at a larger Bragg spacing than the wall thickness and 40 Å will be an overestimate.

The first model of the envelope profile contained a bilayer profile for the cell membrane and, centered 145 Å away, a simple profile for the wall; the envelope profile was identical to the solid curve in Fig. 7*a* except that the "inner protein layer" was absent. The squared Fourier transform of the simplified bilayer profile by itself approximated the low-angle diffraction pattern from the red membrane. The wall was represented by a layer of uniform, ellipsoidal protein molecules; the full width at half maximum of the corresponding inverted-parabola profile is 40 Å for molecules 60 Å long in the direction through the wall. The inverted-parabola shape was simplified as shown by the "outer protein layer" in Fig. 7*a*. The computed diffraction pattern contained peaks and troughs at about the spacings observed.[4] However, for no choice of the height of the wall profile were the relative amplitudes of the peaks and troughs in agreement with Fig. 2. We were therefore obliged to reconsider the model.

Two alternative modifications were suggested by electron micrographs. In micrographs of isolated envelopes (45), the wall material often appears to extend outward from the membrane surface as a broad layer of uniform density. However, the X-ray diffraction peaks and troughs predicted from the corresponding profile were in still worse agreement with the observed pattern, and this alternative structure was rejected. The second alternative was suggested by micrographs of intact cells (43, 45). In these, the outer of the two dark lines locating the cell membrane often appears heavier than the inner one. This appearance led us to consider an additional layer of protein right at the surface of the membrane, which brought the predicted X-ray diffraction into fairly good agreement with the observed pattern, as follows.

Adding an inner protein layer adjacent to the cell membrane (Fig. 7*a*) adds a second cross-interference term of the form of expression (1) to the diffraction, but the diffraction peaks are farther apart than for the outer protein layer since S is smaller (see Fig. 1 in reference 6). Adding an inner layer of protein about half as thick as the outer layer brought the calculated diffraction pattern (Fig. 7*b*) into reasonable agreement with Fig. 2. Thus, the principal parts found for the envelope are the cell membrane and two layers of protein. The protein layers are separated by a broad layer with an electron density close to that of BS. The heights of the two protein profiles, compared to the peaks in the bilayer membrane, indicate that the protein is farily densely packed in both layers. The dashed curves in Fig. 7 are discussed below.

The Patterson function computed from the model profile diffraction is shown by the dashed

[3] For example, a hypothetical structure having the purple membrane in a separate layer parallel to the red membrane could not account for the envelope diffraction in Fig. 2 since similar, nearly symmetric, bilayer profiles are indicated by the diffraction patterns of these two membranes. Similarly, the apposed cell membranes of neighboring envelopes could not account for the peaks and troughs.

[4] The profile and the computed diffraction are shown in Fig. 2 of reference 6.

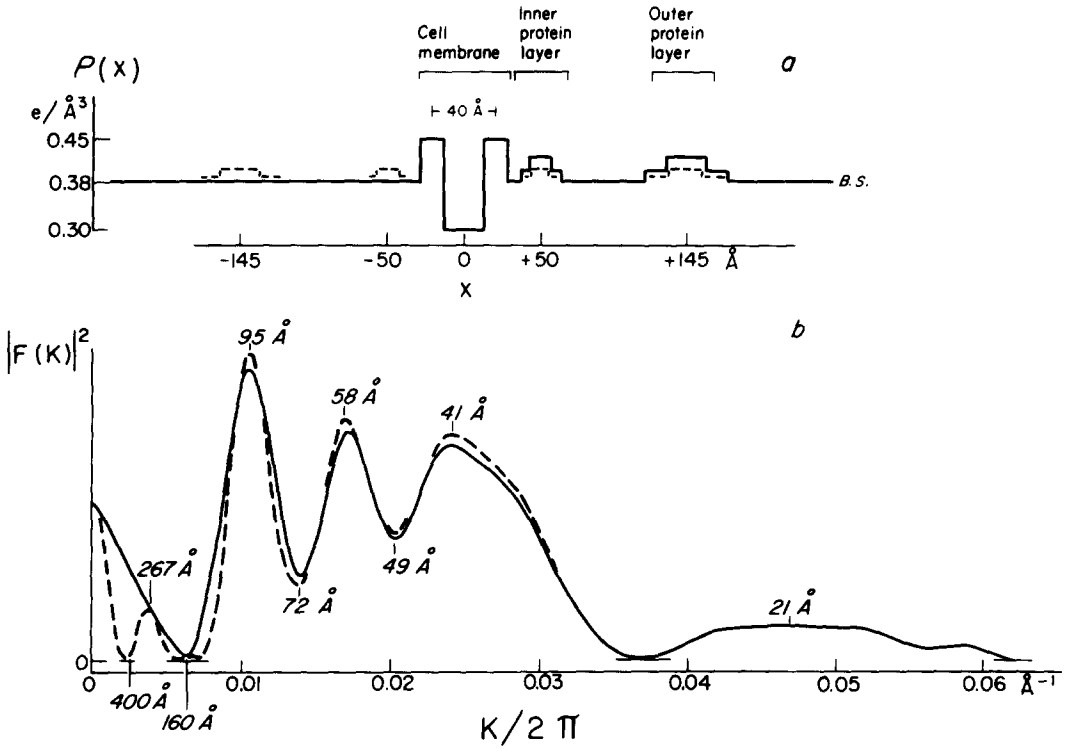

FIGURE 7 Model for the isolated envelope. (*a*) Simplified profile (——) for the cell membrane and the two layers of protein outside. The dashed curve (----) shows the symmetric arrangement of the protein from both layers. (*b*) Corresponding squared Fourier transforms. The series of peaks and troughs in the solid curve can be compared to Fig. 2; $k/2\pi$ is equivalent to R, and $|F(k)|^2$ is equivalent to $I_R R^2$.

curve in Fig. 6. The dashed curve shows, as it must, a form similar to the solid curve, but some differences are apparent. The peak at 177 Å in the model Patterson function is more prominent than the shoulder at 165 Å in the observed Patterson function. This difference mirrors a similar difference in the region of 40–45 Å, suggesting that the model bilayer profile needs some modification. Instead of refining the model, however, a profile has been computed directly from the observed envelope pattern (see below).

We have found several related profiles which are predicted to give similar though not identical diffraction patterns. Thus, the dashed curve in Fig. 7*a* includes the same membrane profile as the solid curve but has the material in the two protein layers arranged symmetrically on the two sides of the membrane. The corresponding diffraction patterns are shown in Fig. 7*b*. The solid and dashed curves are strikingly similar beyond 0.01 Å^{-1}.[5] The main difference is a trough in the dashed curve at about 400 Å, which is absent from the solid curve and which defines a peak at 267 Å. If the inner protein layer is entirely on one side and only the material in the outer layer is arranged symmetrically; or if the outer protein layer is entirely on one side and only the material in the inner layer is arranged symmetrically; or if the inner protein layer is located on the opposite side of the membrane from the outer layer, then a similar peak is predicted. There is no sign of such a peak on the X-ray photographic films, confirming the asymmetry evident in electron micrographs of the envelope in cross section. The overall similarity of the two diffraction patterns in Fig. 7*b* allows us to confirm the envelope profile in a way which

[5] The two squared transforms are very similar because each layer of protein contributes mainly to a cross-interference ripple of the form of Eq. 1. Because Eq. 1 varies linearly with W and depends only on $|S|$, the net result is the same whether the protein is all on one side, at +S, or else distributed equally (or in any other proportions) at $\pm S(6)$.

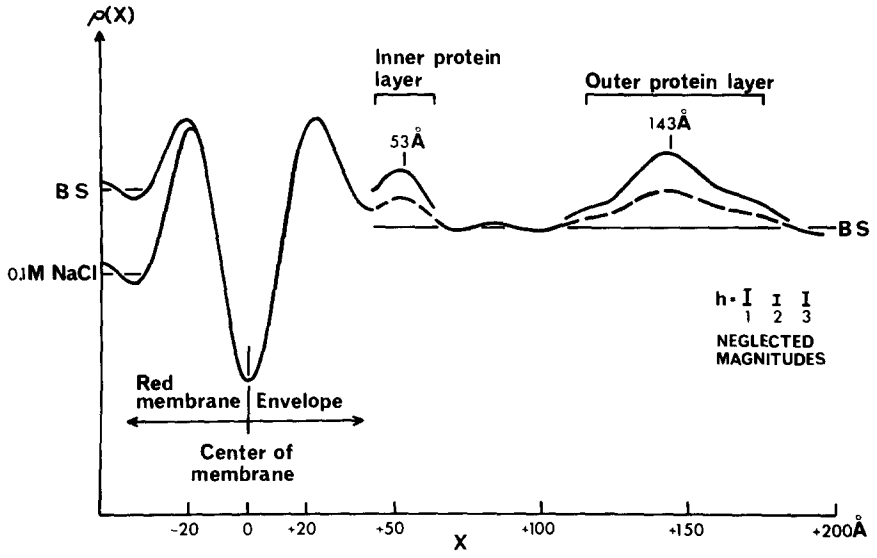

FIGURE 8 The approximate profile calculated for the envelope. A period of 393 Å was chosen in order to calculate the profile, and the magnitudes of the first three orders (h = 1-3) were neglected (see text). To the right of the bilayer cell membrane are two peaks identified as layers of protein. The two peaks in the original, symmetric Fourier synthesis (----) have been doubled in height, relative to the fluid layer between, to correct for the known asymmetry. The space between the two layers of protein is tentatively identified as a periplasmic space (see Discussion).

is to a good extent independent of the model, as follows.

A CALCULATED PROFILE FOR THE ENVELOPE: Assuming that the cell membrane dominates the low-angle envelope pattern, an approximation to the envelope profile can be calculated using the magnitudes observed (square roots of the corrected intensities in Fig. 2) and phase angles for the diffraction from the cell membrane alone.[6] To do the calculation, magnitudes were taken from Fig. 2 for $0.01\ Å^{-1} < R < 0.034\ Å^{-1}$. Magnitudes for $R < 0.01\ Å^{-1}$ were taken as zero since they could not be phased independently of the model and since ignoring them has only a minor effect (see below). For $0.01\ Å^{-1} < R < 0.034\ Å^{-1}$, the same phase angle, π, was assumed as for the symmetric bilayer profile of the red membrane in BS. The calculated envelope profile was then corrected for the fact that the wall lies only to one side of the cell membrane. The resultant profile is shown to the right of the origin in Fig. 8.

In Fig. 8, half of the symmetric approximation to the profile of the cell membrane is shown to the right of the origin. The trough at the center of the membrane locates lipid hydrocarbon chains because they are the only constitutent less electron dense than BS. The peak at +23 Å, and its mirror image at −23 Å (not shown), are identified with electron-dense lipid headgroups. For comparison, halves of the two symmetric profiles of the red membrane are shown to the left of the origin. The profile of the red membrane in BS has much the same form as the cell membrane profile, but the peak in the latter profile is about 1 Å farther from the origin.

Other prominent peaks in the symmetric envelope profile are located at +53 Å and +143 Å, shown by the dashed lines, and at −53 Å and −143 Å (not shown). These are identified as protein layers because, in our preparations, only lipid and protein have been found in large amounts and all of the lipid is in the cell membrane (see Biochemical Analysis). The two protein layers have full widths at half maximum of about 40 Å (outer layer) and 20 Å (inner layer). They are separated by a region with an average level similar to that of the BS in the red membrane profile. The small peak in the region between the two protein peaks is identified with the false detail to be expected in an imperfectly resolved uniform layer (compare the asymmetric model profile in Fig. 7*a* with its

[6] There is an analogy with respect to the case of a dominant heavy atom in a molecule which is discussed by R. E. Dickerson (reference 17, p. 619).

Fourier synthesis in Fig. 9). Assuming that the protein layers lie only to one side of the cell membrane, both dashed peaks in Fig. 8 were doubled in height to derive the final, asymmetric profile. At the same time, the symmetrically related peaks at −53 Å and −143 Å need to be reduced to the level between them. These corrections are justified below.

Approximate profiles have been similarily calculated using magnitudes computed from some models having the same bilayer membrane profile and various wall profiles. In each case, the corresponding wall profile could be distinguished in the Fourier synthesis. Thus, the two peaks to the right of the membrane in Fig. 8 are due in a direct way to the observed magnitudes and are not determined by the phase angles. The approximate envelope profile (Fig. 8) therefore confirms the three parts derived for the model structure.

The accuracy of the approximations used to calculate the asymmetric envelope profile in Fig. 8 have been tested by repeating the calculations on the diffraction pattern predicted from the model envelope profile of Fig. 7. The results show that no large errors are introduced, as follows.

Two Fourier syntheses were calculated, both using the same magnitudes taken from the solid curve in Fig. 7*b* out to 0.036 Å^{-1}. On the one hand, the solid curve in Fig. 9 was calculated using the phase angles computed from the asymmetric model profile, i.e. the solid curve shows the asymmetric model profile to a resolution of 13 Å. On the other hand, the approximate, symmetric synthesis indicated by the open circles in Fig. 9 was calculated using the constant phase angle π since this is the value computed from the cell membrane profile alone. For the approximate synthesis, magnitudes at Bragg's law spacings greater than 100 Å ($k/2\pi < 0.01$ Å^{-1}) were taken as zero because the two computed diffraction curves in Fig. 7*b* diverge there. To complete the approximation, the original protein-layer peaks to the right of the cell membrane in the symmetric synthesis have been doubled in height, giving the open triangles in Fig. 9. The shapes of the approximate profiles of the bilayer (○) and the two layers of protein (△) all agree reasonably well with their counterparts in the solid curve.

In Fig. 9, the parts of the envelope in the approximate synthesis are slightly above or below the respective parts in the solid curve. This is so because the magnitudes taken as zero to calculate the approximate synthesis are coefficients of cosine terms with wavelengths greater than 100 Å. Such terms vary too slowly to have much effect on the shapes of the three parts but can raise or lower any of them. Since the same approximations were made to compute the envelope profile in Fig. 8, the electron density in the space between the two protein layers is not known very accurately. Therefore, although the density is approximately that of BS, the space could contain small amounts of undetected proteins. The same inaccuracy helps to explain the higher level for the BS outside the red membrane as compared to the level in the envelope profile.

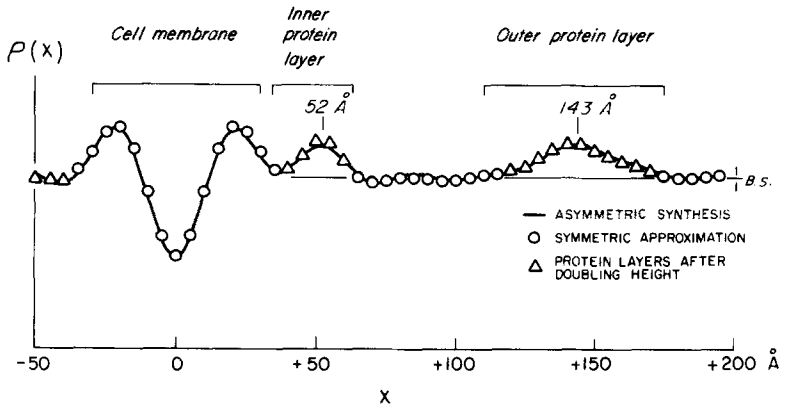

FIGURE 9 Fourier syntheses approximating the model profile of Fig. 7. The open circles (○) show the approximate profile using the same phase angles as for the membrane alone; the open triangles (△) show the protein peaks after doubling them. These approximations are the same as for Fig. 8. The solid curve (——) shows the exact, asymmetric model profile at the same resolution.

Electron Microscopy

The appearance of the cell wall and membrane in sectioned and shadowed preparations of whole cells and isolated envelopes has been reported previously (45). We now correlate these results with the new data obtained by X-ray diffraction and add a few observations on the membrane and envelope fractions obtained by the modified procedures.

We have not detected any significant differences in the fine structure of envelopes (E-BS) prepared by freezing and thawing rather than by shaking with glass beads. The same regular array of particles first described by Houwink (21) can be seen in shadowed preparations, and a cell wall on the outer surface of a unit membrane can be distinguished in sections. Also, the membrane vesicles prepared in buffered 20 mM $MgSO_4$ (E-Mg) are not obviously different from those prepared by diluting in BS to 1.0 M NaCl (Fig. 10), except that more of the E-Mg vesicles appear to be broken, and somewhat less dense material appears to adhere to both surfaces of the membrane. This may be attributed, at least in part, to the greater number of centrifugation and resuspension steps in their preparation. The envelopes in 2 M salt (E-2.0) appear more disorganized than in the earlier preparations obtained by simply diluting BS to 2.0 M NaCl content. E-0.1/EDTA and E-H_2O contain mainly broken vesicles, and a considerable amount of very small membrane fragments and some amorphous material are found in the upper part of the pellet.

In cross sections of the 150-Å thick layer found outside of the cell membrane, an inner light zone can often be observed (15, 45). An interpretation of the light zone in the sectioned and stained preparations was not possible. This finding, however, takes on a new significance now that the model based on X-ray diffraction shows a space of lower electron density in the wall. The electron micrographs apparently reflect the distribution of protein in the cell wall.

An aqueous space has also been detected by freeze-etching. The 4.3 M NaCl concentration in the growth medium or BS effectively acts as a cryoprotectant, and no ice crystal formation is usually observed in freeze-fractured preparations. The high salt concentration, like other cyroprotectants, also prevents effective etching, and the actual surface of the cell envelope with its ordered structure is rarely revealed by freeze-etching. However, as Fig. 11 shows, prolonged etch times allow the removal of some ice and lower the level of the frozen saline surface slightly. Cross fractures through the cell envelope then become visible and reveal a line of depression between the membrane and the outer protein layer of the envelope. This depression is identified by its location and by the etching effect as the space in envelopes which is observed by X-ray diffraction to have a lower electron density and which appears light in electron micrographs of sectioned bacteria. It is etched to approximately the same depth as the surrounding saline and should therefore largely contain saline.

In tangential fractures through the envelopes of whole bacteria or isolated envelope (E-BS), the fracture appears to occur within the membrane. It reveals two fracture faces similar in appearance to those seen in many other cell membranes (12). In whole bacteria, the two fracture faces are easily identified with the inner lamella and outer lamella of the cell membrane by their curvature (the inner fracture face is convex, the outer concave) and by their spatial relation to the cell wall when the latter is revealed by etching. The inner fracture face carries a high concentration of small round particles, with an apparent size of 40 Å to 90 Å. The outer fracture face shows much fewer particles, and some of them are slightly larger in size (Fig. 11). The purple membrane, when it is present, can be recognized as patches of different texture (10). We found essentially the same features in the fracture faces at lower salt concentrations; however, below 2.0 M NaCl, it became necessary to add other cyroprotectants, which inhibited etching even more effectively than BS.

Biochemical Analysis

FRACTIONATION OF THE ENVELOPE: It was shown in the earlier work (44, 45) that when the envelope preparation in BS is diluted to a final concentration of 1 M NaCl, cell wall material is lost from the envelope vesicles and is largely recovered as soluble protein in the colorless supernate. Most of the cell membrane material in the red 50,000 *g* sediment is still in the form of membrane-bounded vesicles, with possibly residual cell wall material attached (see Electron Microscopy). When the supernate is further fractionated on a Sephadex G75 column equilibrated with BS diluted to 1 M NaCl and eluted with the same solvent, some red material, presumably small cell

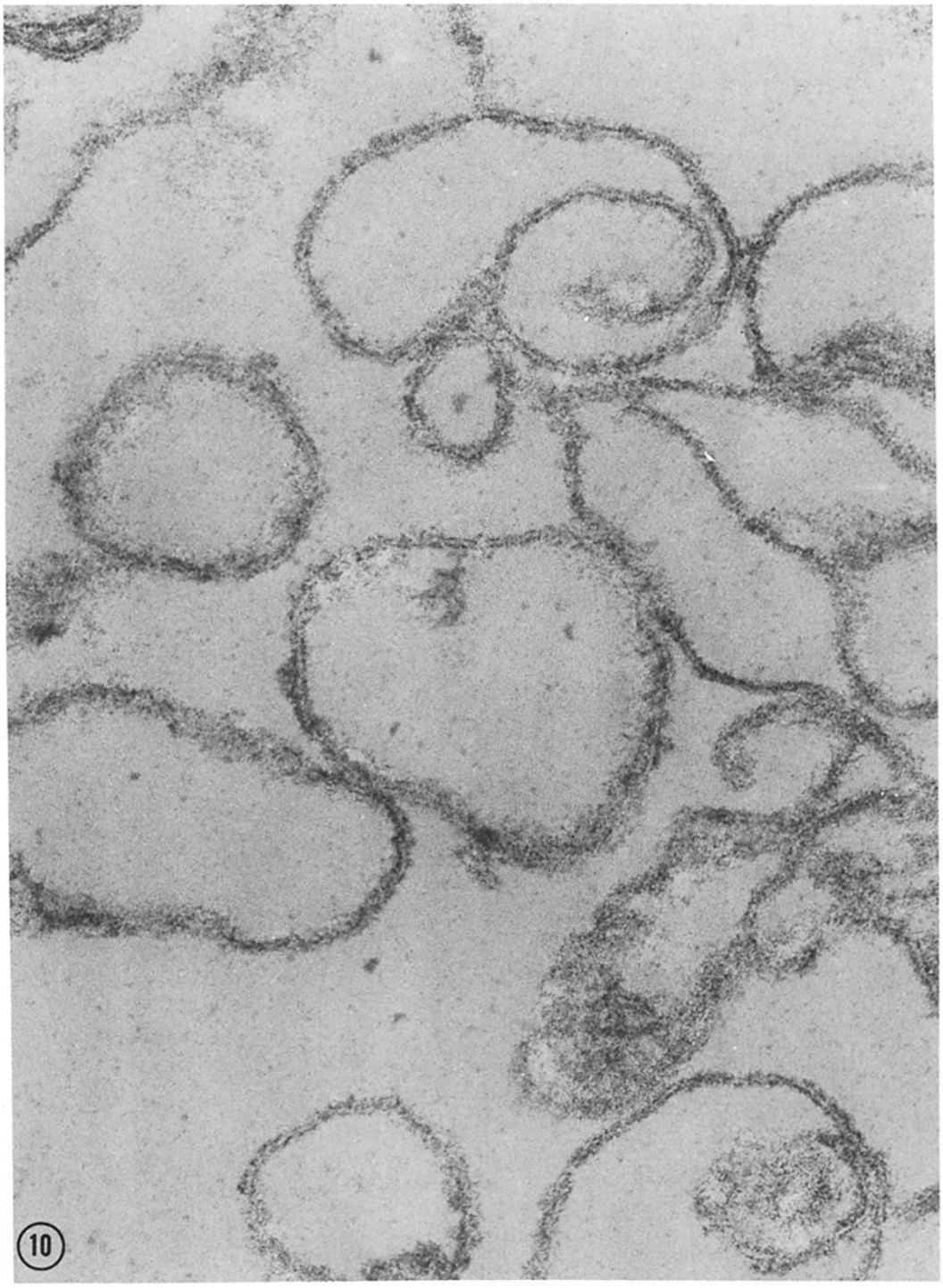

FIGURE 10 Membrane vesicles prepared in buffered 20 mM $MgSO_4$ (E-Mg). The triple-layered membrane structure is clearly visible. No remaining wall material is seen on the membrane surface. × 154,000.

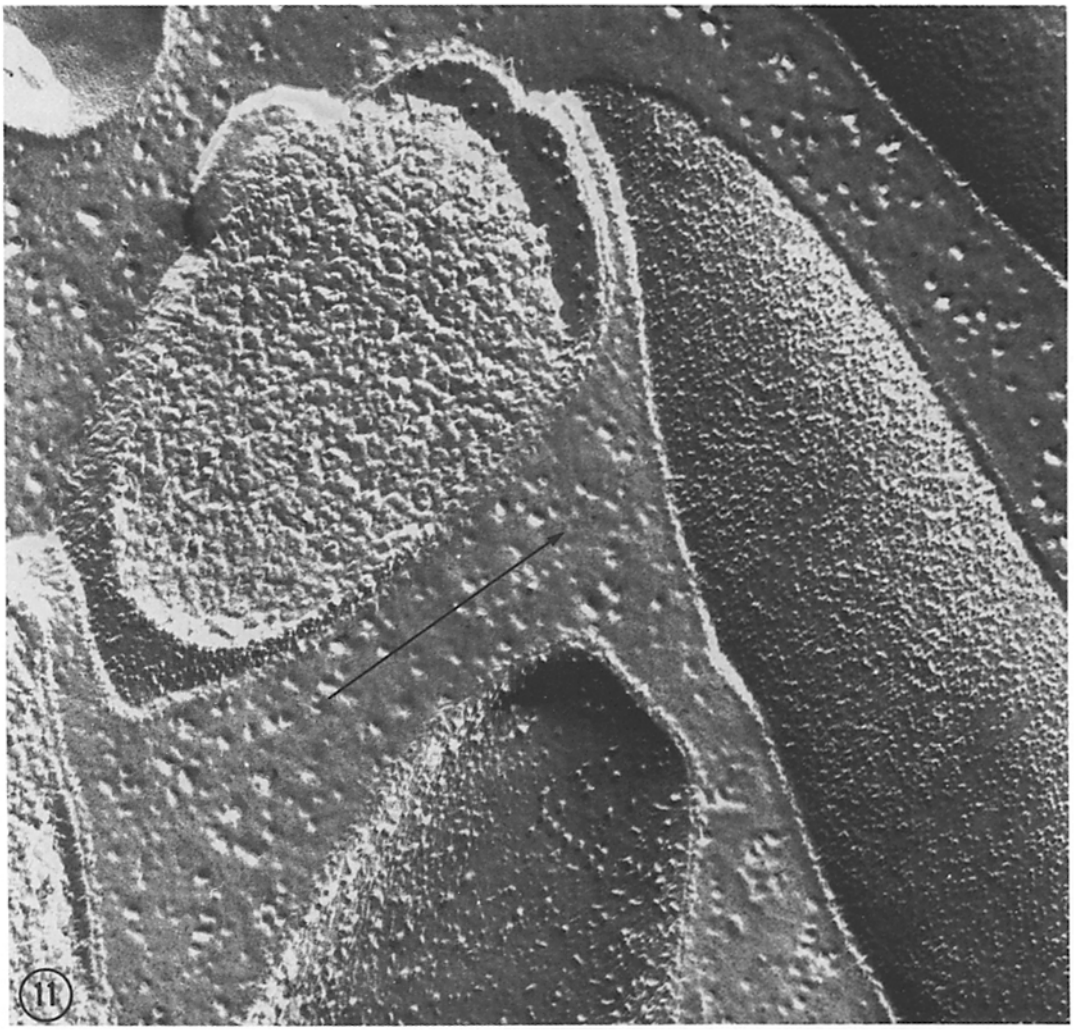

FIGURE 11 Freeze-etch preparation of *H. halobium*. The convex inner fracture face and the concave outer fracture face show the typical particle distributions. As seen at the edges of the concave fractures, the wall appears split by a depression which is not visible without extensive etching, indicating the periplasmic space. × 82,200.

membrane fragments, and some colorless aggregates appear in the void volume. Repeated, prolonged sedimentation removes most of the red material but not the colorless material from this supernate. The void volume material is followed by two colorless peaks at Kd = 0.27 and Kd = 0.73 (Fig. 12). Analytical ultracentrifugation after removal of the large aggregates also shows two peaks; the main peak has a S_{20} = 1.6 independent of salt concentration between 1.0 and 0.1 M NaCl. This, as well as a Kd value of 0.73, indicates a molecular weight between 10,000 and 20,000. SDS disc gel electrophoresis (46) of this fraction shows two main bands with apparent mol wt of 16,000 and 21,000 and several minor bands of higher apparent molecular weight (Fig. 13).

When the NaCl concentration of the cell envelope fraction is reduced below 1.0 M NaCl by dilution with water, the membrane vesicles begin to break up into smaller nonvesicular fragments (45). If, however, the Mg^{++} concentration is kept constant at 20 mM while the NaCl concentration is reduced, the NaCl may be removed completely without extensive fragmentation of the membrane

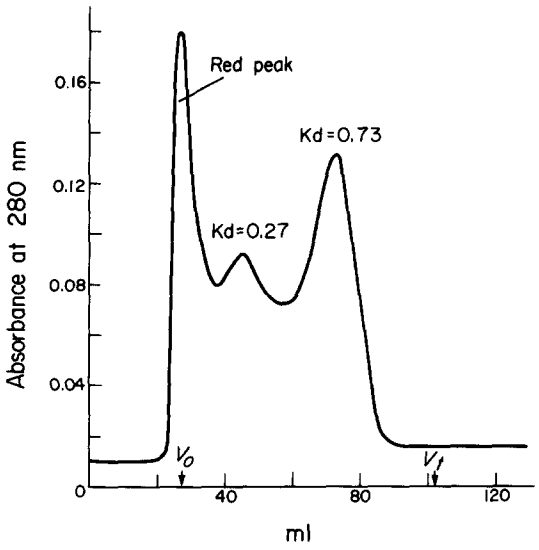

FIGURE 12 Sephadex G75 in BS 1:4.3 with H_2O.

vesicles. An analysis of the supernates and sediments obtained at different NaCl concentrations in the presence of 20 mM $MgCl_2$ is shown in Fig. 14. Because no N-containing lipids are found in *H. halobium* (23) and because the envelopes contain only negligible amounts of nucleic acids (44), the N values of the fractions reflect the protein content and the P values (3) the lipid content. As can be seen from Fig. 14, the composition of the envelopes is essentially unchanged when the NaCl concentration is lowered from 4.3 M to 2.0 M. Between 2.0 and 1.0 M, about half the protein is lost from the envelopes and recovered in the supernate, whereas the lipid content is reduced by only 20%. These data agree with earlier results (44, 45) showing a dissociation of cell wall in this range of salt concentrations. The 20% loss of lipid may be attributed to small fragments of membrane which are released when the wall dissociates. However, because 20 mM Mg^{++} is present in these preparations below 1.0 M NaCl concentration, no further protein or lipid is lost from the sediment.

Electron microscopy of the pellets from E-0.1 to E-Mg shows mostly membrane-bounded vesicles without cell wall. Some of the vesicles have apparently been broken as indicated by the presence of membrane sheets.

CsCl density gradient centrifugation of the pellets shows that the loss of protein from the envelopes results in a decrease in buoyant density. E-BS and E-2.0 show the same position in the gradient, and the density decreases progressively from E-2.0 to E-1.0; between E-1.0 and E-Mg, there is no further significant decrease in density.

FRACTIONATION OF MEMBRANE VESICLES: Fraction E-0.1 is sedimented and resuspended in 0.1 M NaCl containing 0.1 M EDTA (and no $MgCl_2$) at pH 7.0 and then dialyzed against the same solution. This treatment leads to a dissociation of the membrane vesicles, and centrifuging for 5 h at 300,000 *g* separates the components into a colorless supernate over a yellow viscous layer and a red pellet (E-0.1/EDTA). The pellet contains the red and purple membrane fragments which can be separated as described elsewhere (see Materials and Methods and references 35, 37). The colorless supernatant after concentration and the yellow fraction both show the same sedimentation pattern in the analytical ultracentrifuge (Fig. 15), one band with rather strongly concentration-dependent S values. Extrapolation yields $S^0_{20,w} = 5.9 \times 10^{-13}$ s (Fig. 16), and a diffusion coefficient $D^0_{20,w} = 2.2 \times 10^{-7}$ (cm^2/s) has been determined. Centrifugation in a CsCl gradient yields a buoyant density of 1.33 g/cm^3,

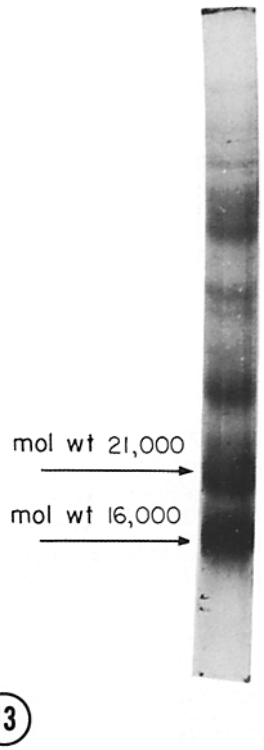

FIGURE 13 SDS gel from E-1.0.

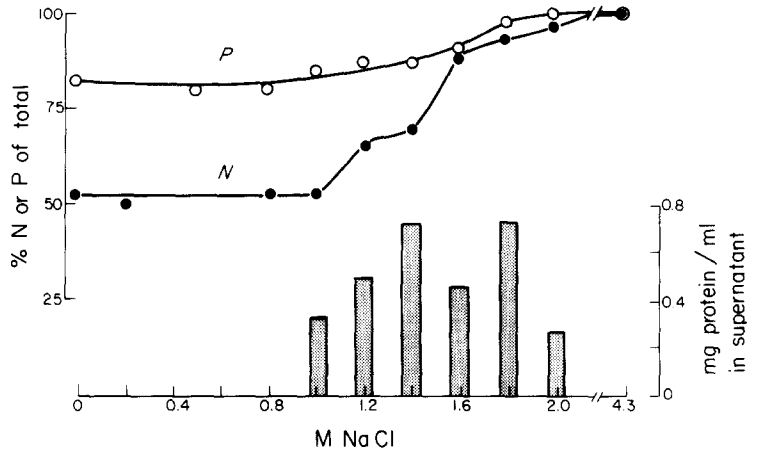

FIGURE 14 Percent nitrogen or phosphorus; mg/ml protein in supernate.

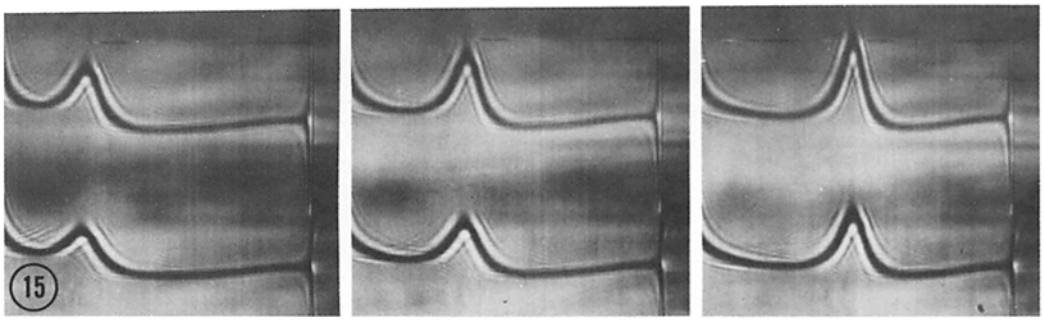

FIGURE 15 Analytical ultracentrifugation of supernate from EDTA-treated fraction E-0.1. Upper trace: 10 mg/ml protein. Lower trace: 7 mg/ml protein. Solvent: 0.1 M NaCl containing 10 mM EDTA, pH 7.3; 60,150 rpm; sedimentation from right to left 80, 96, and 112 ms from start; no faster moving material was observed.

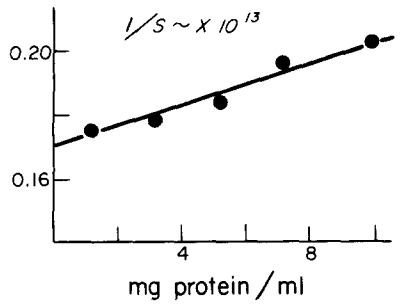

FIGURE 16 Concentration dependence of S values for the yellow protein fraction.

typical for a protein. The partial specific volume has not been determined. SDS disc gel electrophoresis indicates a more complex composition, with one major band of apparent mol wt of 110,000 and at least 10 minor bands.

Similar fractions are obtained when membrane vesicles (E-1.0) are dialyzed against distilled water instead of 0.1 M NaCl + 0.1 M EDTA. The fragments of the membrane are smaller in this case and, even after prolonged centrifugation, small amounts of lipid, protein and pigment can still be found in the supernate. In a typical experiment, after a 27-h run at 150,000 g the faintly reddish supernate was concentrated and showed one main and two minor peaks in the ultracentrifuge. The sedimentation velocity of the main peak was strongly concentration dependent and extrapolated to $S^0_{20,w} = 7.3 \times 10^{-13}$ s. It may be identical to the material in the yellow fraction obtained by EDTA extraction, and the different S value may be the result of running in water instead of buffered NaCl solutions. However, the fraction obtained by water extraction is clearly more heterogeneous. This is indicated also by preliminary results from density gradient centrif-

ugation and acrylamide disc gel electrophoresis. Difference and fluorescence spectra indicate that it contains cytochromes and flavin(s).

DISCUSSION

The Periplasmic Space

The cell envelope of *H. halobium* had already been shown to include a cell membrane and a cell wall with a highly ordered surface. We have now resolved two layers, consisting predominantly of protein, outside the cell membrane. A substantial fluid space separates the two protein layers. This space is tentatively identified with the "periplasmic space" of gram-negative bacteria.

A periplasmic space has been postulated in the envelope of gram-negative bacterial cells to explain how a number of soluble proteins can be selectively released by osmotic shock or other procedures which leave the cell membrane permeability barrier intact but disturb the cell wall (20, 32, 39). The released proteins ("periplasmic proteins") are detected by their enzymatic activities or their specific binding of low molecular weight substrates which are subsequently transported into the cell. The periplasmic proteins appear not to be bound to any component of the cell envelope although cytochemical tests indicate that they are present in the cell periphery. In intact cells, they are accessible to their substrates but not to specific antibodies. However, the cytochemical data do not allow an exact localization of the periplasmic proteins (47).

The periplasmic space in the envelope of *H. halobium* is best defined by the X-ray results: a space 65 Å wide on the average with approximately the electron density of the surrounding basal salt solution and located between two layers of protein. Ice is removed from this space in the freeze-etch preparations, confirming a high proportion of saline there. A layer of low density is often seen in electron microscope sections of the envelope. Although it demonstrates only that little or no heavy metal stain is bound in this layer, this observation is consistent with an aqueous space. More to the point, the variable appearance in the micrographs (sometimes the low density layer is filled in by a broad layer of stain) is explained by assuming that in some preparations the wall structure becomes disordered and spreads into the fluid space. The data presented here appear to be the first to demonstrate directly a layer fulfilling the structural requirements for a periplasmic space in a bacterial cell.

No periplasmic proteins have yet been demonstrated in any of the halobacteria. However, these may be among the minor components found in the disc gel electrophoresis of protein released from *H. halobium* cell envelopes when the salt concentration is lowered from BS to 1.0 M (Fig. 13). It should be interesting to study the release of proteins from envelopes and from whole cells with this question in mind.

The Two Protein Layers

The general structure of the envelope of *H. halobium,* a cell membrane with a presumably rigid wall outside, is similar to that of the envelopes of nonhalophilic bacteria (19). However, the unique chemical composition requires that some functions common to both halobacteria and other procaryotic cells are carried out by chemically different materials in halobacteria.

The outer permeability barrier in gram-negative bacteria apparently resides in a lipopolysaccharide layer. This layer is absent from halobacteria. Instead, there is an outer protein layer which is clearly a barrier, but with pores of unknown size. The inner protein layer may also be a barrier.

The maintenance of shape in other bacteria is commonly attributed to a murein (peptidoglycan) layer (31, 42). This layer also is absent from *H. halobium,* and we can only assume that the outer protein layer plays an essential part in this function. A regular beading can be seen in EM cross sections of the outer layer, confirming the crystalline structure indicated by the highly ordered cell surface (21, 43, 45). The crystalline structure strongly suggests that the outer protein layer is rigid. The X-ray results also favor the outer layer in so far as it is thicker than the inner protein layer and hence may be stronger. Moreover, when the ionic strength of the suspension medium is gradually lowered, the bacteria develop irregular shapes (1, 33) in the range where the X-ray observations indicate that the envelope structure is disturbed. Then, the outer protein layer breaks up at a point where the cells become spheres or disappear altogether. The inner layer is not eliminated from consideration, however, since the X-ray observations indicate that it also is lost at NaCl concentrations below 2.0 M (cf. Fig. 4 here with Fig. 1 in reference 6).

The function of the inner protein layer is not known. It may be part of the wall since a dense 20 Å-thick layer of protein is in general not found on the surface of isolated cell membranes (5, 6). It cannot be decided from the existing electron micrographs and X-ray data whether the inner layer has a regular arrangement in the plane, as would be expected for a purely structural role. A decisive proof that the inner layer is part of the wall would be to prepare viable protoplasts from which this layer has been removed. However, a different technique for its selective removal must be found since the low ionic strength used here invariably kills the cells and is likely to cause irreversible changes in protein conformation. It remains to relate the peculiarities of chemistry and structure to the unique environment in which halobacteria exist.

Similarities between H. halobium and Other Halobacteria

The electron optical morphology of *H. halobium* cell envelopes appears to be very similar to the morphology observed in other species of halobacteria (27, 33, 43), and much the same low-angle X-ray diffraction pattern has been recorded from envelopes (E-BS) of *H. salinarium* and *H. cutirubrum* (Blaurock, unpublished observations; Dr. W. Wober cultured the cells and prepared the envelopes).

The chemistry of *H. halobium* cell envelopes also appears to be very similar to that of other species of halobacteria (27, 33, 43). The disaggregation of the envelope occurs in a very similar fashion. Only the maximal salt concentration at which it begins may differ somewhat in different species (38, 43). We note that culture conditions have been reported to affect the susceptibility to lysis in low salt of at least one strain (1). Immunological studies emphasize the close relationship between the different strains (49).

The Cell Membrane

The cell membrane in *H. halobium* broadly resembles other cell membranes. It appears as a unit membrane in electron micrographs of sectioned material. The particle populations on the inner and outer fracture faces show a density and size distribution similar to that seen in other cell membranes. The protein composition is complex, including firmly bound cytochromes and flavoproteins. The low-angle X-ray diffraction pattern of the red membrane is similar to that observed for several other biological membranes (48). Diffraction at 10 Å, identified with the protein, shows the in-plane orientation (Blaurock, unpublished observation) observed for other membranes (9, 11).

Our evidence for a bilayer membrane includes a bilayer-like image in the Patterson function for the envelope. Changes in the X-ray diffraction pattern when the red membrane is transferred from water to basal salts confirm the bilayer interpretation. The red membrane pattern indicates two similar, narrow layers 40 Å apart. This distance is close to the values derived from other membrane patterns (48), and the same distance is indicated by the X-ray diffraction patterns from both the extracted lipids and the purple membrane (9, 10).

Approximate, symmetric profiles computed for the red membrane and its parent cell membrane in the envelope show the two electron-dense layers and a region of low density between. The two dense layers are identified with the lipid headgroups in two layers. Lipid hydrocarbon chains must be present in the region between the two layers to account for the low density.

The solution to the problem of arranging the lipid and protein in the red membrane has been carried further by comparing its X-ray diffraction pattern with that from the extracted lipids dispersed in water (9). The two patterns are clearly distinguished: although broad diffraction bands are observed at similar spacings, the first intensity minimum in Fig. 4*a*, at 0.01 $Å^{-1}$, is considerably farther from the origin than the first minimum in the lipid pattern (8). This comparison indicates that the red membrane protein is not all located outside a normal lipid bilayer; rather, much of the protein must be inserted into the bilayer (5, 6, 8). Comparison of the two calculated profiles shows the greater density in the core of the red membrane. In support of this arrangement, the freeze-cleave pictures show particles on both fracture faces.

The particle populations on the two faces differ in number and size distribution, indicating an asymmetric structure. A somewhat asymmetric structure proposed for the purple membrane (9) has more of the protein, and correspondingly less of the lipid, on one side of the center of the membrane than on the other. A similar structure will account for the red membrane X-ray diffraction pattern, but this model for the asymmetry remains to be confirmed.

We thank Miss Jill Hill for preparing cells and envelopes; Mr. Z. Gabor for prints of the X-ray patterns; and Mr. Istvan Marot for help with the freeze-fracturing and freeze-etching experiments.

This work was supported by National Heart and Lung Institute program project grant HL 06285.

Received for publication 3 September 1974, and in revised form 26 May 1976.

Note Added in Proof: In a recent paper on the "Purification and characterization of a prokaryotic glycoprotein from the cell envelope of *Halobacterium salinarium*" (*J. Biol. Chem.* 1976. **251**:2005–2014), Mescher and Strominger describe a glycoprotein of apparent mol wt of 200,000. This protein accounts for about half of the protein of the cell envelope. We note that EM of the envelope of the halobacteria (21, 43, 45) shows particles in a hexagonal array in what we now call the outer protein layer. The rows of particles are about 130 Å apart, center to center. This dimension defines a hexagonal unit cell of area 19,500 Å^2; assuming that the outer protein layer is 40 Å thick, the volume of the unit cell is 780,000 Å^3. Assuming, as the above authors suspect, that the glycoprotein is in the outer protein layer and taking a protein density of 1.33 g/cm^3 (9), the unit cell can contain just over three molecules. A cluster of three molecules therefore will account for the particle size seen by EM. A threefold rotation axis at the center of each cluster will account for the hexagonal packing as well. Any excess unit-cell volume, above that actually occupied by the three molecules, can reasonably be assigned to one or more pores through the outer protein layer. Such pores will be needed in order for metabolites to pass through the wall. (Note added June 30, 1976.)

REFERENCES

1. ABRAM, D., and N. E. GIBBONS. 1960. Turbidity of suspensions and morphology of red halophilic bacteria as influenced by sodium chloride concentration. *Can. J. Microbiol.* **6**:535.
2. ABRAM, D., and N. E. GIBBONS. 1961. The effect of chlorides of monovalent cations, urea, detergents, and heat on morphology and the turbidity of suspensions of red halophilic bacteria. *Can. J. Microbiol.* **7**:741.
3. BARTLETT, G. R. 1959. Phosphorus assay in column chromatography. *J. Biol. Chem.* **234**:466.
4. BLAUROCK, A. E. 1971. Structure of the nerve myelin membrane: proof of the low-resolution profile. *J. Mol. Biol.* **56**:35.
5. BLAUROCK, A. E. 1972. Locating protein in membranes. *Nature (Lond.).* **240**:556.
6. BLAUROCK, A. E. 1973. X-ray diffraction pattern from a bilayer with protein outside. *Biophys. J.* **13**:281.
7. BLAUROCK, A. E. 1973. The structure of a lipid-cytochrome c membrane. *Biophys. J.* **13**:290.
8. BLAUROCK, A. E. 1973. Locating protein in membranes. *Nature (Lond.).* **244**:172.
9. BLAUROCK, A. E. 1975. Bacteriorhodopsin: a trans-membrane protein containing α-helix. *J. Mol. Biol.* **93**:139.
10. BLAUROCK, A. E., and W. STOECKENIUS. 1971. Structure of the purple membrane. *Nat. New Biol.* **233**:152.
11. BLAUROCK, A. E., and M. H. F. WILKINS. 1969. Structure of frog photoreceptor membranes. *Nature (Lond.).* **223**:906.
12. BRANTON, D. 1969. Membrane structure. *Annu. Rev. Plant Physiol.* **20**:209.
13. BRINTON, C. C., JR., J. C. MCNARY, and J. CARNAHAN. 1969. Purification and in vitro assembly of a curved network of identical protein subunits from the outer surface of a *Bacillus. Bacteriol. Proc.* 48 GP30 (Abstr.).
14. BROWN, A. D. 1963. The peripheral structures of gram-negative bacteria. IV. The cation-sensitive dissolution of the cell membrane of the halophilic bacterium, *Halobacterium halobium. Biochim. Biophys. Acta.* **75**:425.
15. CHO, K. Y., C. H. DOY, and E. H. MERCER. 1967. Ultrastructure of the obligate halophilic bacterium *Halobacterium halobium. J. Bacteriol.* **94**:196.
16. DANON, A., and W. STOECKENIUS. 1974. Photophosphorylation in *Halobacterium halobium. Proc. Natl. Acad. Sci. U. S. A.* **71**:1234.
17. DICKERSON, R. E. 1964. X-ray analysis and protein structure. *In* The Proteins. Composition, Structure, and Function. Second Edition. H. Neurath, editor. Academic Press, Inc., New York. **2**:603.
18. FRANKS, A. 1955. An optically focusing X-ray diffraction camera. *Proc. Phys. Soc. London Sect. B.* **68**:1054.
19. GLAUERT, A. M., and M. J. THORNLEY. 1969. The topography of the bacterial cell wall. *Annu. Rev. Microbiol.* **23**:159.
20. HEPPEL, L. A. 1969. The effect of osmotic shock on release of bacterial proteins and on active transport. *J. Gen. Physiol.* **54**:95s.
21. HOUWINK, A. L. 1956. Flagella, gas vacuoles and cell-wall structure in *Halobacterium halobium*; an electron microscope study. *J. Gen. Microbiol.* **15**:146.
22. JAMES, R. W. 1948. The optical principles of the diffraction of X-rays. *In* The Crystalline State. Volume II. W. L. Bragg, editor. G. Bell & Sons, Ltd., London.
23. KATES, M., L. S. YENGOYAN, and P. S. SASTRY. 1965. A diether analog of phosphatidyl glycerophosphate in *Halobacterium cutirubrum. Biochim. Biophys. Acta.* **98**:252.
24. KLUG, A., J. T. FINCH, R. LEBERMAN, and W. LONGLEY. 1966. Design and structure of regular

virus particles. *In* Principles of Biomolecular Organization. G. E. W. Wolstenholme and M. O'Connor, editors. J. & A. Churchill Ltd., London. 158.

25. KONCEWICZ, M. A. 1972. Glycoproteins in the cell envelope of *Halobacterium halobium*. *Biochem. J.* **128:**124P (Abstr.).
26. KONCEWICZ, M. 1972. The presence of a sulphated polysaccharide in the cell envelopes of *Halobacterium halobium*. *Biochem. J.* **130:**40P (Abstr.).
27. KUSHNER, D. J., S. T. BAYLEY, J. BORING, M. KATES, and N. E. GIBBONS. 1964. Morphological and chemical properties of cell envelopes of the extreme halophile, *Halobacterium cutirubrum*. *Can. J. Microbiol.* **10:**483.
28. KUSHNER, D. J., and H. ONISHI. 1968. Absence of normal cell wall constituents from the outer layers of *Halobacterium cutirubrum*. *Can. J. Biochem.* **46:**997.
29. LANYI, J. K. 1971. Studies of the electron transport chain of extremely halophilic bacterium. VI. Salt dependent dissolution of the cell envelope. *J. Biol. Chem.* **246:**4552.
30. MARSHALL, C. L., A. J. WICKEN, and A. D. BROWN. 1969. The outer layer of the cell envelope of *Halobacterium halobium*. *Can. J. Biochem.* **47:**71.
31. MARTIN, H. H. 1969. Die struktur der zellwand bei gramnegativen bakterien. Arzneim-Forsch. *Drug Res.* **19:**266.
32. MITCHELL, P. 1961. Approaches to the analysis of specific membrane transport. *In* Biological Structure and Function. Vol. II. T. W. Goodwin and O. Lindberg, editors. Academic Press, Inc., New York. 581.
33. MOHR, V., and H. LARSEN. 1963. On the structural transformations and lysis of *Halobacterium salinarium* in hypotonic and isotonic solutions. *J. Gen. Microbiol.* **31:**267.
34. MOOR, H., and K. MÜHLETHALER. 1963. Fine structure in frozen-etched yeast cells. *J. Cell. Biol.* **17:**609.
35. OESTERHELT, D., and W. STOECKENIUS. 1971. Rhodopsin-like protein from the purple membrane of *Halobacterium halobium*. *Nat. New Biol.* **233:**149.
36. OESTERHELT, D., and W. STOECKENIUS. 1973. Functions of a new photoreceptor membrane. *Proc. Natl. Acad. Sci. U. S. A.* **70:**2853.
37. OESTERHELT, D., and W. STOECKENIUS. 1974. Isolation of the cell membrane of *Halobacterium halobium* and its fractionation into red and purple membrane. *In* Methods in Enzymology-Biomembranes. S. Fleischer, L. Packer and R. Estabrook, editors. Academic Press, Inc., New York. **31:**667.
38. ONISHI, H., and D. J. KUSHNER. 1966. Mechanisms of dissolution of envelopes of the extreme halophile *Halobacterium cutirubrum*. *J. Bacteriol.* **91:**646.
39. PARDEE, A. B. 1968. Membrane transport proteins. *Science (Wash. D. C.).* **162:**632.
40. RACKER, E., and W. STOECKENIUS. 1974. Reconstitution of purple membrane vesicles catalyzing light-driven proton uptake and adenosine triphosphate formation. *J. Biol. Chem.* **249:**662.
41. RAND, R. P., and V. LUZZATI. 1968. X-ray diffraction study in water of lipids extracted from human erythrocytes. The position of cholesterol in the lipid lamellae. *Biophys. J.* **8:**125.
42. ROGERS, H. J. 1970. Bacterial growth and the cell envelope. *Bacteriol. Rev.* **34:**194.
43. STEENSLAND, H., and J. LARSEN. 1969. A study of the cell envelope of the halobacteria. *J. Gen. Microbiol.* **55:**325.
44. STOECKENIUS, W., and W. H. KUNAU. 1968. Further characterization of particulate fractions from lysed cell envelopes of *Halobacterium halobium* and isolation of gas vacuole membranes. *J. Cell. Biol.* **38:**337.
45. STOECKENIUS, W., and R. ROWEN. 1967. A morphological study of *Halobacterium halobium* and its lysis in media of low salt concentration. *J. Cell Biol.* **34:**365.
46. WEBER, K., and M. OSBORN. 1969. The reliability of molecular weight determinations by dodecyl sulfate-polyacrylamide gel electrophoresis. *J. Biol. Chem.* **244:**4406.
47. WETZEL, B. K., S. S. SPICER, H. F. DVORAK, and L. A. HEPPEL. 1970. Cytochemical localization of certain phosphatases in *Escherichia coli*. *J. Bacteriol.* **104:**529.
48. WILKINS, M. H. F., A. E. BLAUROCK, and D. M. ENGELMAN. 1971. Bilayer structure in membranes. *Nat. New Biol.* **230:**72.
49. ZWILLING, B. S., R. ROWEN, and G. STOTZKY. 1969. Immunological relationships among some species of extremely halophilic bacteria. *J. Bacteriol.* **98:**384.